THE JOURNAL OF PHYSICAL CHEMISTRY C

C: Surfaces, Interfaces, Porous Materials, and Catalysis

Why Citrate Shapes Tetrahedral and Octahedral Colloidal Platinum Nanoparticles in Water

José M Gisbert-Gonzalez, Juan M. Feliu, Adolfo Ferre-Vilaplana, and Enrique Herrero

J. Phys. Chem. C, **Just Accepted Manuscript** • DOI: 10.1021/acs.jpcc.8b05195 • Publication Date (Web): 26 Jul 2018

ACS Publications

is published by the American Chemical Society. 1155 Sixteenth Street N.W., Washington, DC 20036

Why Citrate Shapes Tetrahedral and Octahedral Colloidal Platinum Nanoparticles in Water

José M. Gisbert-González[a], *Juan M. Feliu*[a], *Adolfo Ferre-Vilaplana*[b]*, *and Enrique Herrero*[a]*

[a]Instituto de Electroquímica, Universidad de Alicante, Apdo. 99, E-03080 Alicante, Spain. [b]Instituto Tecnológico de Informática, Ciudad Politécnica de la Innovación, Camino de Vera s/n, E-46022 Valencia, Spain, and Departamento de Sistemas Informáticos y Computación, Escuela Politécnica Superior de Alcoy, Universidad Politécnica de Valencia, Plaza Ferrándiz y Carbonell s/n, E-03801 Alcoy, Spain.

Corresponding Authors
*e-mail: aferre@dsic.upv.es and herrero@ua.es

Abstract

The performance of many advanced catalytic systems depends not only on the size and composition but also on the specific shape of the metal nanoparticles (NPs) from which they are assembled. In turn, the shape of colloidal NPs depends on the specific capping agent involved in their synthesis, though the mechanism is still poorly understood. Here, supported by electrochemical experiments, FTIR spectra and DFT calculations, on well-defined surfaces, we show how a specific capping agent determines the shape of colloidal NPs. Solvated citrate can become simultaneously adsorbed on the Pt(111) surface through three dehydrogenated carboxylic groups, each one of them in bidentate configuration. On the other basal planes, citrate is adsorbed through only two of them. For this reason, under the synthesis conditions, citrate is more favorably adsorbed on the Pt(111) than on the other two basal planes of platinum. This adsorption behavior explains why colloidal platinum NPs of tetrahedral and octahedral shape are produced when citrate is used as the capping agent in water. The mechanism for citrate would also operate determining the shape of other pure fcc metals and can inspire the engineering of future capping agents.

1. Introduction

The performance of catalytic processes, such as those involved in electrochemical synthesis and fuel cells, depends on the way in which the desired reactions are favored on the accessible surfaces of key materials (the catalysts). These are usually composed of expensive and scarce pure metals and their alloys. Thus, to maximize the exposed surface for a given load of catalyst, metal nanoparticles (NPs) have been widely used in the most advanced catalytic systems. [1–7] In turn, the catalytic performance of metal NPs (activity and selectivity toward the target reaction) depends, in general, not only on their size and composition, but also on their specific shape, determined by the nature of the crystalline surfaces (the combination of terraces, steps, edges and defects) that they expose. For this reason, the effective application of the NPs approach to the optimization of catalysts is not a trivial task. On one side, the nature of the most active NPs (composition, size, and shape) has to be determined. On the other side, methods allowing the synthesis of the NPs, not only with the desired composition but also with the preferred size and shape, must be fine-tuned.[8,9] As a counterpart, the NPs approach broadens enormously the design space for a catalyst, being currently considered an essential resource to solve the most challenging problems in sustainable chemistry and energy development. In the limit, the quantum effects, which emerge when small enough NPs (clusters) are approached, have to be specifically addressed and exploited.

Thus, numerous efforts have been aimed to control not only the size but also the shape of metal NPs produced by colloidal synthesis.[10,11] To achieve the desired control, capping agents, such as polyvinylpyrrolidone (PVP),[12] hexadecyltrimethylammonium bromide (CTAB)[13,14] or citrate[15] have been extensively used in these processes. It is generally accepted that solvated capping agents are preferentially adsorbed on certain surfaces of the growing crystals, during the synthesis process, selectively limiting the relative growth rate of each

specific face, and eventually controlling the final shape of the produced NPs. So, for a given composition (via precursors) and synthesis conditions, the capping agent would determine the shape of the obtained NPs. Therefore, the ability of engineering specific capping agents for the synthesis of any desired NP of a specific shape would represent a major breakthrough in the area. Although the relationship between capping agents and NPs shapes has been previously investigated,[8,9] it is still poorly understood even for the most frequently used capping agents and metals due to inherent research difficulties. Among these, two of them can be emphasized. First, colloidal processes of synthesis are not, in general, very reproducible because the resulting products depend on the accurate control of several parameters (such as precursors, temperature, pH or even purity of the capping agents), which is not always experimentally achievable. And, second, the detailed adsorption behavior of solvated species on the surfaces of particles in suspension cannot be directly established. In any case, a more in-depth knowledge of the mechanisms determining not only the size by also the shape of NPs seems essential in order to engineer future capping agents.

Because citrate can be easily removed from many metal surfaces, which is essential to activate their catalytic properties, it has been extensively used as a capping agent. Citrate for gold NPs is by far the most investigated capping agent,[16–23] though the mechanism is not still known in detail. Due to the fact that platinum is a much more relevant electrocatalyst, the relationship between citrate used as a capping agent and the shape of the colloidal platinum NPs to which gives rise to in water is here considered. It is known that, under certain conditions, citrate gives rise to platinum NPs of tetrahedral and octahedral shape in water,[16,24] but the mechanism is still poorly understood. On conducting materials, several aspects of the adsorption behavior of species on surfaces can be explored by means of electrochemical experiments. In fact, the adsorption of solvated citrate on polycrystalline electrodes of platinum in water has been investigated by Electrochemical Quartz Crystal Microbalance

(EQCM),[25] and Time-of-Flight Secondary Ion Mass Spectrometry (*TOF-SIMS*) and XPS techniques.[26] However, since adsorption properties are, in general, very dependent on the specific surface and site, only when well-defined surfaces are used in research, adsorption process on crystals, and how they operate during colloidal synthesis, can be completely understood. Additional features regarding adsorption processes, which are essential to untangle the mechanisms, can be obtained from DFT calculations. Here, using a strategic combination of electrochemical experiments, FTIR spectra and DFT calculations, on well-defined surfaces, the adsorption behavior of solvated citrate on the basal planes of platinum (Pt(111), Pt(100) and Pt(110)) in water, under different solvation conditions, are for the first time established. Because on the Pt(111) electrode hydrogen and OH adsorptions in water take place at different potential windows, a full thermodynamic analysis of the adsorption properties of solvated citrate on this surface can be carried out from electrochemical experiments following the method previously applied to sulfate.[27] However, since under electrochemical conditions in water the Pt(110) surface reconstructs,[28] and on the Pt(100) and Pt(110) surfaces the hydrogen and OH adsorption processes are competitive,[29,30] the approach followed for the Pt(111) electrode cannot be applied to these surfaces. Elements of the adsorption behavior of citrate on the Pt(100) and Pt(110) surfaces will be experimentally established by comparison with the adsorption behavior of analogs to citrate on the different basal planes of platinum. The reported electrochemical results under different citrate concentrations and pH conditions, complemented by FTIR spectra and DFT calculations, provide insights explaining why citrate as capping agent gives rise to colloidal platinum NPs with preferential tetrahedral and octahedral shape under certain conditions in water.

2. Methods

Platinum single crystal electrodes were prepared from spherical single crystal beads obtained after the controlled fusion of a 0.5 mm diameter high purity platinum wire.[31] The beads were mounted in a four-circle goniometer on an optical bench, oriented using the reflections of a laser, cut and polished along the desired orientation (miscut below 0.1º). Prior their use, they were flame annealed, cooled down in a reductive atmosphere (hydrogen + argon) and protected with a droplet of water in equilibrium with the atmosphere. It has been shown that this procedure leads to surfaces with the lower number of defects.[32] The absence of the peaks at 0.125 and 0.27 V, related to the presence of defects and steps on the surface, and the sharp peak at 0.8 V in 0.1 M $HClO_4$ are characteristics of a well ordered surface, with a miscut in the order of the nominal value.

A glass cell equipped with a platinum counter electrode was used in all cases. For solutions with pH<3, a reversible hydrogen electrode (RHE) was used as a reference, whereas, in the remaining solutions, the reference was measured versus an Ag/AgCl electrode. In this latter case, the electrode potentials were converted to the RHE for comparison. Cyclic voltammograms were recorded at ν=50 mV s^{-1}, using a wave signal generator (EG&G PARC 175), a potentiostat (eDAQ 161), and a digital recorder (eDAQ e-corder 401). All experiments were performed at room temperature.

IR experiments were performed with a Nicolet Magna 850 spectrometer equipped with a MCT (Mercury–Cadmium–Telluride) detector. In this type of experiments, the cell has a prismatic CaF_2 window beveled at 60º. 100 interferograms were collected for each spectrum with a resolution of 8 cm^{-1}. P- and s-polarized light were used to discriminate between solution and adsorbed species. The spectra are plotted as $-\log(R_1-R_2/R_1)$, where R_2 and R_1 represent the reflectance values corresponding to the spectra recorded at the sample and reference potentials. The formation of new species at the sample potential (or the increase in

their concentration) gives rise to the appearance of positive bands in the spectra, whereas the negative bands are associated with a diminution of the concentration of the species.

Solutions were prepared using Elga Purelab Ultra water (18.2 MΩ cm resistivity), $HClO_4$ (Merck Suprapur), citric acid (Sigma-Aldrich ≥99.5%), sodium citrate (Sigma-Aldrich ≥99%), NaF (Sigma-Aldrich 99.99%). Solutions were deoxygenated using with Ar (N50, Air Liquide).

All DFT calculations were carried out using numerical basis sets,[33] semi-core pseudopotentials [34] (which include scalar relativistic effects) and the PBE[35] and RPBE[36] functionals as implemented in the Dmol^3 code[37]. When considered, dispersion forces were corrected by the Tkatchenko and Scheffler method.[38] Continuous solvation effects were taken into account by the COSMO model.[39] The effects of non-zero dipole moments, in the supercells, were canceled by means of external fields.[40] Proton-coupled electrons transfers were modeled by means of the computational hydrogen electrode formalism.[41]

Being specifically developed for catalysis, it is generally assumed that RPBE provides a better description of adsorption on transition metals than PBE. In fact, it is known that PBE systematically over-bind regarding RPBE. Moreover, due to the size of the investigated adsorbate, it can be anticipated that the effect of the dispersion forces could become significant. However, the treatment of the dispersion forces under the RPBE functional is not supported by the aforementioned software package. In order to obtain results under the RPBE functional with dispersion forces, dispersion corrected estimations under the PBE functional were in turn corrected by the difference between calculations under the PBE and the RPBE functionals, both of them without considering the effect of the dispersion forces. Constant lattices were specifically estimated for each numerical treatment, that is, PBE, RPBE, and PBE-D, and the corresponding one was used in the assembling of each model.

The Pt(111), Pt(100) and Pt(110) surfaces were modeled by means of periodic supercells comprising 48 Pt atoms (four layers of metal atoms) and a vacuum slab of 20 Å. The bottom 24 Pt atoms were frozen in their bulk crystal locations, meanwhile the remaining 24 Pt atoms were completely relaxed joint to the adsorbates. The shortest distance between periodic images was in the order of 8.50 Å for all the models. Additional details, about the computational methods, are provided in the Supporting Information.

3. Results and Discussion

3.1. Citrate adsorption on platinum from experiments.

3.1.1. *Citrate adsorption on the Pt(111) electrode*

To explore the adsorption behavior of citrate on the Pt(111) surface, voltammetric profiles for this electrode in 0.1 M $HClO_4$ under different concentrations of citric acid in solution are displayed in Figure 1. The pH was maintained constant throughout the experiment by adding citric acid as a reactant. The presence of citrate in solution leads to the disappearance of adsorption states above 0.6 V, which are associated with the OH adsorption on the Pt(111) electrode in perchloric acid solution.[42] Moreover, new adsorption states between 0.3 and 0.6 V appear upon the addition of citric acid, which are connected to citrate adsorption on the electrode. The hydrogen adsorption profile between 0 and 0.3 V is not affected by the presence of citrate. However, a small overlap between the adsorption/desorption process of hydrogen and citrate takes place between 0.3 and 0.4 V, giving rise to the formation of a small peak at 0.34 V for low citrate concentrations. This peak is linked to the competitive hydrogen/citrate adsorption/desorption process. As the citric acid concentration increases, the citrate adsorption states shift to lower potential values, increasing the overlap between both processes. As a result, the peak at 0.34 V shifts to lower potential values and increases its intensity.

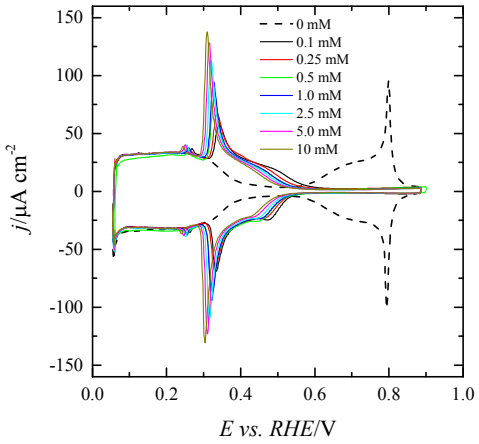

Figure 1. Voltammetric profiles of Pt(111) electrodes in solution at 0.1 M $HClO_4$(pH=1.2) under different concentrations of citric acid. Scan rate: 50 mV s^{-1}.

Using the electrocapillary equation for the Pt/solution interface as starting point,[43] the voltammetric profiles obtained under different citric acid concentrations allow to determine the Gibbs excesses of citrate adsorbed on the Pt(111) electrode, as has been already done for sulfate,[44,45] chloride,[46,47] or phosphate[48] (Complete details for the calculation of these excesses are provided in the Supporting Information). These surface excesses as a function of the charge are plotted as Figure 2A. Note that the specific nature of the adsorbed species (citrate, monohydrogen citrate, or dihydrogen citrate) cannot be determined from thermodynamic considerations only. Thus, the calculated values correspond to the accumulated excess of the three adsorbed species. From this plot, and using the potential vs. surface charge density for a given concentration displayed as Figure S1A, plots for the surface excess vs. electrode potential can be constructed (Figure 2B). As can be seen, the onset of the adsorption of citrate species is ca. 0.3 V and the maximum surface excess is ca. 3.0×10^{14} ions cm^{-2}. This number corresponds to a surface coverage of 0.20, whose value is the same as that obtained for sulfate[44,45,49,50] or phosphate[48] on this electrode.

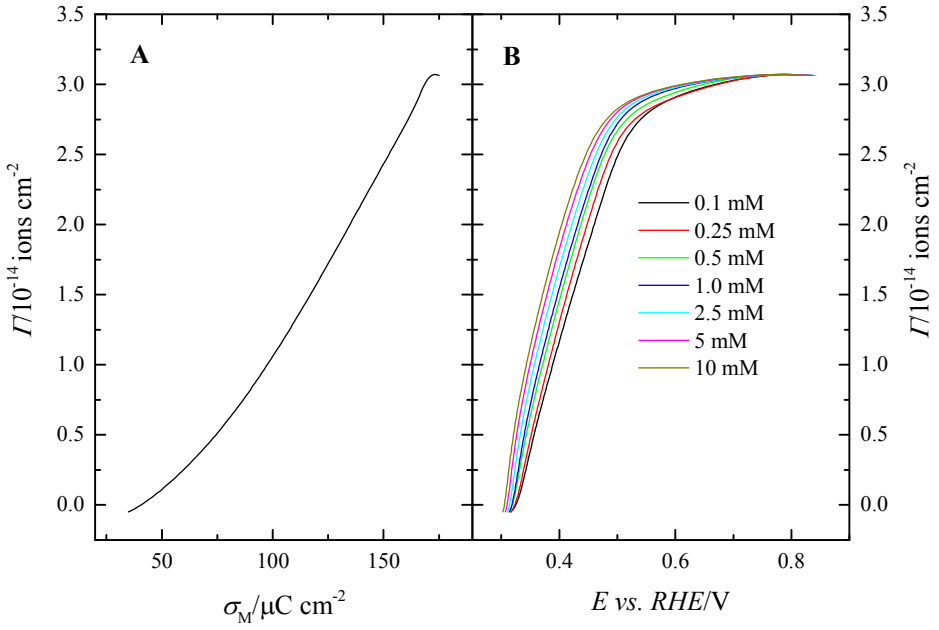

Figure 2. Surface excess for citrate adsorbed on the Pt(111) electrode vs. A) surface charge density and B) electrode potential for 0.1 M $HClO_4$ solutions.

Although the specific nature of the adsorbed species cannot be determined from thermodynamic results only, the number of electrons flowing through the circuit per adsorbed species (charge numbers) can provide some insight into the subject. Two different charge numbers can be calculated from the cross differential of the electrocapillary equation:[51] the formal partial charge at constant electrode potential l, usually known as electrosorption valency, and the charge number at a constant chemical potential n', which is the reciprocal of the Essin-Markov coefficient (details about the calculation of these charge numbers are provided in the Supporting Information). Both charge numbers vs. charge and electrode potential are displayed as Figure 3. These charge numbers are between 3 electrons per ion at low coverages and 2 when the adlayer reaches the saturation, suggesting that the adsorbed species are citrate and monohydrogen citrate. Therefore, the adsorption reactions would be:

$$Pt+C_6H_8O_7 \rightarrow Pt\text{-}C_6H_5O_7+3H^++3e^- \quad (1)$$

and

$$Pt+C_6H_8O_7 \rightarrow Pt\text{-}C_6H_6O_7+2H^++2e^- \quad (2)$$

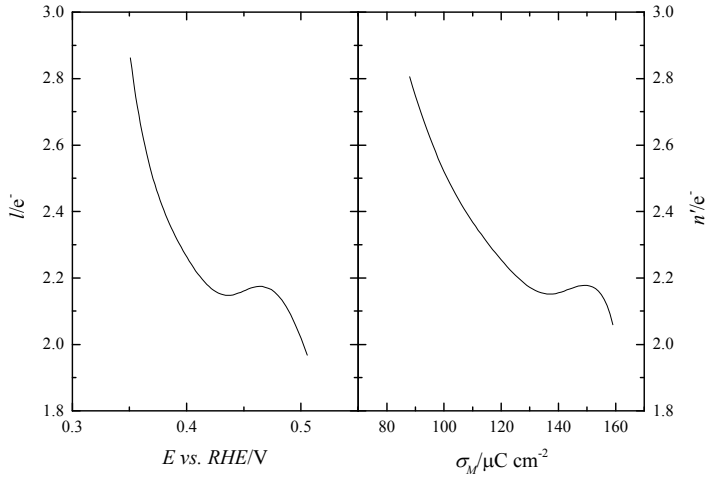

Figure 3. Charge numbers (*l* and *n'*) obtained according to equations S6 and S7, respectively.

Thus, the major adsorbed species are deprotonated, although the predominant species in solution is the acid form. This evidence suggests that adsorbed citric acid behaves as a stronger acid, with pK_a values of the adsorbed species significantly smaller than that corresponding to the species in solution. A similar behavior has been observed for other cases, such as sulfate or carbonate,[50,52] whose pK_a for the adsorbed species is significantly smaller. The observed behavior in acid indicates that citrate would be the only species adsorbed on the surface irrespectively of the pH.

Additional insights into the nature of the adsorbates can be obtained from pH-dependent studies. If the adsorption process occurs according to the reactions (1) and (2) the equilibrium potential should shift 59 mV per pH unit, which implies that in the RHE scale, the adsorption process should occur at a constant potential. Note that the reactions (1) and (2) are only valid when citric acid is the main species in solution (that is, pH<3.13). For the pH range between 3.13 and 4.76, where dihydrogen citrate is the main species in solution, the adsorption reactions would be:

$$Pt+C_6H_7O_7^- \rightarrow Pt\text{-}C_6H_5O_7+2H^++3e^- \quad (3)$$

and

$$Pt+C_6H_7O_7^- \rightarrow Pt\text{-}C_6H_6O_7+1H^++2e^- \quad (4)$$

and thus, the equilibrium potential should shift 40 or 30 mV per pH unit, respectively. Therefore, in the RHE scale, the adsorption process should shift to higher potential values. To verify this behavior, voltammetric profiles at different pH values were measured (Figure 4). By using mixtures of NaF and $HClO_4$, the pH was maintained constant during each experiment due to the buffering capacity of the HF/F^- acid-base equilibria (pK_a=3.17).[53] It can be observed in Figure 4 that for pH<3.13 the voltammetric profiles are almost independent of the pH. On the other hand, for pH=4.3 (Figure 4C) some changes are already detectable. First, there is a slight shift of the adsorption processes to higher potential values and the voltammogram is no longer symmetric with respect to the x-axis. Moreover, a significant shoulder, which is very prominent in the negative scan direction, appears at 0.5 V. This shoulder is especially evident for low citrate concentrations, suggesting an important change in the adsorption process.

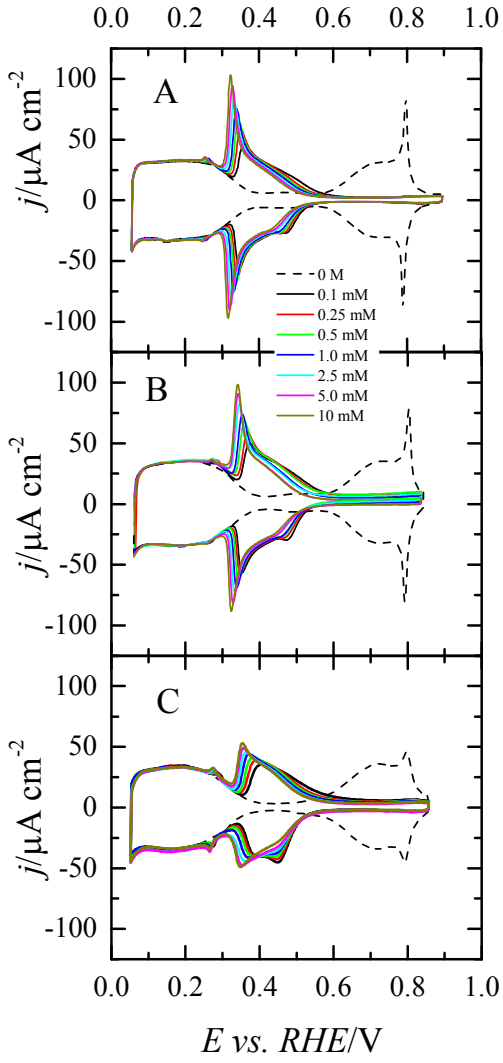

Figure 4. Voltammetric profiles of the Pt(111) electrode in different solutions A) 0.01 M $HClO_4$+ 0.09 M $NaClO_4$ (pH=2.2); B) 2.99×10^{-2} M $HClO_4$+ 4.84×10^{-2} NaF (pH=2.9); and C) 0.028 M $HClO_4$+ 0.2 M NaF (pH=4.3) under different citric acid concentrations. Scan rate 50 mV s^{-1}.

For the solutions with pH<3.13, the thermodynamic analysis of the data is possible, since the voltammograms are symmetrical. Using the procedure previously used, surface excesses and charge numbers were estimated under different pH conditions (Figures 5 and 6). Excesses for citrate are almost pH independent, which confirms that, in the citrate adsorption process, the number of exchanged protons and electrons is the same. On the other hand, charge numbers are slightly higher for pH>2, corroborating the conclusion for pH=1.2 that the pK_a values for the adsorbed species are significantly lower than those measured for the

species in solution. For pH=1.2, as the coverage increases, the number of electrons exchanges diminishes, suggesting that at high coverages the main adsorbed species is monohydrogen citrate. However, as pH increases, the major adsorbed species is citrate for the whole of the coverage range.

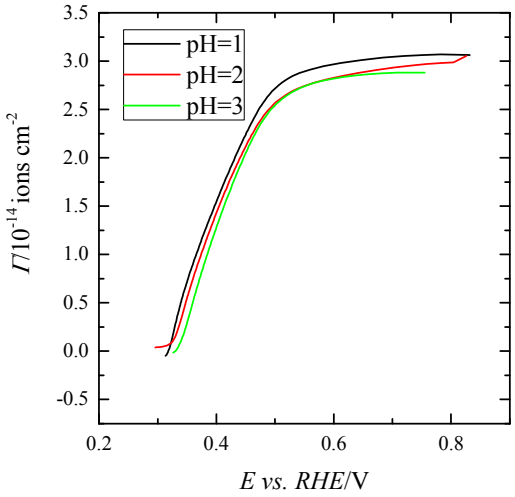

Figure 5. Surface excesses for citrate vs. electrode potential in different pH solutions with 1 mM citric acid.

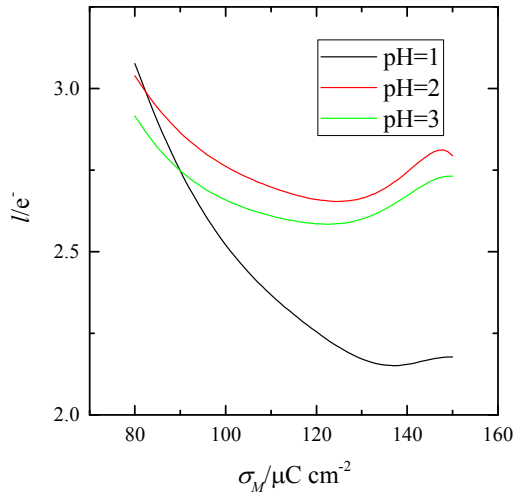

Figure 6. Charge number (l) calculated for adsorbed citrate in different pH solutions with1 mM citric acid.

These results for the Pt(111) electrode are very similar to those reported for Au(111).[54,55] In fact, the maximum coverage obtained for adsorbed citrate on both metals is the same for pH<pK_a (3.0×10^{14} ions cm^{-2}). Additionally, the calculated charge numbers for

the adsorption process are also very similar, ranging between 2 and 3.[54,55] The only minor difference is that the charge numbers close to the saturation coverage increase to values close to 3 on the Au(111) electrode. For the Pt(111) electrode, the completion of the adlayer occurs at the same potential as the onset of OH adsorption in perchloric acid solutions. Therefore, the thermodynamic analysis for E>0.55 V leads to an underestimation of the charge transfer values. From the initial state in perchloric acid solution to the final state in citrate containing solution at E>0.55 V, there is a reductive desorption of OH and an oxidative adsorption of citrate, so that the overall electron transfer is smaller than that taking place in a surface free from adsorbed OH.

FTIR experiments provide additional information on the nature of the adsorbed species. The spectra evolution with the electrode potential for the Pt(111) electrode in acidic solutions containing citric acid is displayed as Figure 7. The spectrum acquired at 0.05 V was used as reference because no citrate was detected at this potential. Two major bands can be appreciated: one in the region between 1700-1650 cm^{-1} and other one centered at 1412 cm^{-1}. The first band corresponds to the water bending mode and is related to the movement of water molecules in and out the thin gap between the prism and the electrode as potential changes. From complementary spectra and location, the second band can be related to adsorbed citrate. Owing to the selection rules, adsorbed species are not visible to the s-polarized light. This second band is not present when the spectra are taken with s-polarized light (obtained but not shown). Therefore, it is clearly related to adsorbed species. Being located at the onset of citrate adsorption (around 0.4 V), the band should be related to adsorbed citrate. In fact, the band at 1412 cm^{-1} can be assigned to the C-O symmetric stretching vibration of the COO group adsorbed on the electrode surface in a bidentate configuration. The same band has been observed for adsorbed acetate on platinum single crystal electrodes.[56] Moreover, a similar band at 1385 cm^{-1} is observed for adsorbed citrate on Au(111), which has been also assigned

to the COO group bonded to the surface in a bidentate configuration.[55] Finally, the small Stark tuning effect of the detected vibrational modes of adsorbed citrate (>10 cm^{-1} V^{-1}) is very similar to that observed for other species in which the COO group is adsorbed in a bidentate configuration such as acetic acid or trifluoroacetic acid.[56,57]

On the other hand, owing to the selection rules of the adsorbed species, only those vibrational modes in which the change of dipole has a component perpendicular to the surface are active in IR for the p-polarized light. Thus, the absence of additional bands related to citrate adsorption suggests that the main chain of the adsorbed species lays parallel to the surface. This condition could be satisfied by citrate being simultaneously bonded to the surface by one, two or even three of the carboxylic groups of the molecule, each one of them in bidentate configuration.

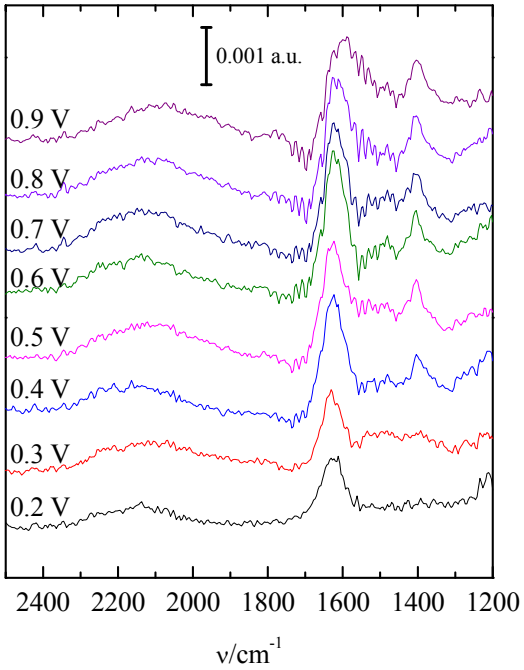

Figure 7. FTIR for the adsorbed species on the Pt(111) electrode in solutions containing 0.1 M $HClO_4$ 10 mM citric acid (pH=1.2) for different electrode potentials.

3.1.2. *Citrate adsorption on Pt(100) and Pt(110) electrodes*.

Because Pt(110) reconstructs in water under electrochemical conditions,[28] and on Pt(100) and Pt(110) the hydrogen and OH adsorption processes are competitive,[29,30] the complete experimental approach used for Pt(111) cannot be applied to Pt(100) and Pt(110). So, absolute coverages and charge transfer numbers cannot be determined for these surfaces. However, a qualitative analysis of the adsorption properties of these planes can be performed by comparison with other adsorbed anions. Voltammograms for Pt(100), Pt(110) and Pt(111) in 1 mM of citric acid, sodium chloride and acetic acid together with the blank voltammogram in perchloric acid are displayed as Figure 8. For the Pt(111) electrode, when the citrate adsorption is compared with that of acetate and chloride two significant insights can be drawn. First, the adsorption of citrate takes place at lower potentials than that of acetate, which means that the first one is stronger. Note that both species are adsorbed through carboxylic groups bonded to the surface in a bidentate configuration. Second, the onsets of the citrate and chloride adsorptions are very similar. However, the completion of the adsorbed layer takes place at more positive potentials for chloride (ca. 0.8 V) vs. citrate (ca. 0.5 V). This fact indicates that adsorbed chloride species should have strong repulsive interactions that hinder the final stages of the adsorption process. Although chloride transfers an electron upon adsorption,[46] the Pt—Cl bond is likely highly polarized, generating strong repulsive interactions among adsorbates, which hinders the formation of a complete adlayer. Conversely, for adsorbed citrate, the possible formation of hydrogen bonds with water stabilizes the adlayer.

For Pt(100) and Pt(110), the presence of specifically adsorbed anions (citrate, acetate or chloride) results in the appearance of well-defined peaks in the voltammograms, which are related to the competitive adsorption of hydrogen and the specifically adsorbed anion. At positive potentials to the peak anions are adsorbed, whereas at negative potentials the surface

is covered by hydrogen. Thus, the position of the peak reflects the interaction strength of the anion with the surface. Therefore, the specific order of interaction strength for the analyzed anions on the different basal planes of platinum is:

Pt(111): Chloride≈citrate>acetate

Pt(100): Chloride>citrate>acetate

Pt(110): Chloride≈citrate>acetate

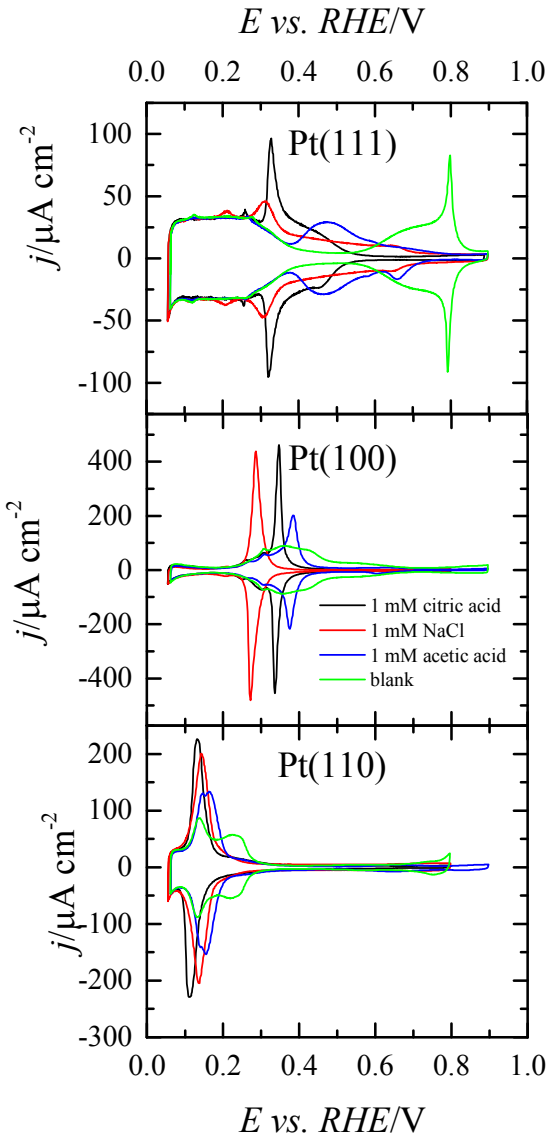

Figure 8. Voltammetric profiles of platinum basal planes at 0.1 M $HClO_4$ with the addition of 1 mM of citric acid, NaCl, and acetic acid. Scan rate: 50 mV s^{-1}.

Additionally, FTIR spectra for adsorbed citrate was recorded for the Pt(100) and Pt(110) electrodes. The measured spectra are very similar to those measured for the Pt(111) electrode and only the bands at ca. 1410 cm^{-1} and those related to water are observed, indicating that the citrate species are boded through the carboxylic groups. The only major difference with the spectra of the Pt(111) electrode is the onset for the detection of the band at 1410 cm^{-1}, which coincides with the onset for citrate adsorption of each electrode.

3.2. Citrate adsorption on platinum from DFT calculations.

Considering the experimentally derived insights regarding citrate adsorption on platinum, chemisorbed states of citrate on the different basal planes of platinum (Pt(100), Pt(110) and Pt(111)), after one, two and three proton-coupled electron transfers (PCETs), with the main chain of the adsorbate laying parallel to the surface and each one of the dehydrogenated carboxylic groups simultaneously bonded to the surface in bidentate configuration, were searched for using DFT. For each significant configuration found, the free energy (ΔG) and the resultant equilibrium potential (E) were calculated using the corresponding electrode reaction:

$$Pt+C_6H_8O_7 \rightarrow Pt\text{-}C_6H_7O_7+1/2\,H_2 \quad (5)$$

$$Pt+C_6H_8O_7 \rightarrow Pt\text{-}C_6H_6O_7+H_2 \quad (6)$$

$$Pt+C_6H_8O_7 \rightarrow Pt\text{-}C_6H_5O_7+3/2\,H_2 \quad (7)$$

The most favorable configurations found after each number of PCETs on each one of the basal planes of platinum are displayed in Table S1, whereas the corresponding energies and electrode potentials are collected in Table 1 (details about energetic calculations are provided in the Supporting Information). Additionally, the most relevant of the obtained chemisorbed states of citrate on the different basal planes of platinum (those binding the

higher number possible of carboxylic groups to the surface in bidentate configuration) are summarized as Figure 9. After a single PCET, chemisorbed states of citrate satisfying the pre-established conditions were found on each one of the basal planes of platinum (Table S1). From Table 1, it can be concluded that these adsorption processes (through a single dehydrogenated carboxylic group bonded to the surface in bidentate configuration after a single PCET) are very favorable on platinum, given that ΔG values are between -0.19 and -0.73 eV, which correspond to equilibrium electrode potentials between -0.19 and -0.73 V, depending on the surface.

After two PCETs, plausible chemisorbed states of citrate satisfying the pre-established conditions were also found on each one of the basal planes of platinum (Table S1 and Figures 9A-B). In Table 1 can be observed that, under electrochemical conditions, citrate can be also adsorbed on platinum through two dehydrogenated carboxylic groups simultaneously, each one of them in bidentate configuration. For the Pt(100) and Pt(110) surfaces, the calculated potentials for these adsorption process are lower than those corresponding to the onset of hydrogen desorption on those planes (ca. 0.20 and 0.1 V, respectively). Thus, citrate must compete with hydrogen for the adsorption sites, giving rise to sharp and intense peaks, as those observed in Figure 8. For the Pt(111) surface, the calculated potential for the onset of citrate adsorption in the bidentate configuration coincides with the final stages of hydrogen desorption (ca. 0.35 V), originating the peak at ca. 0.3 V observed in Figure 1.

Finally, after three PCETs, possible chemisorbed states of citrate satisfying the pre-established conditions were only found on the Pt(111) surface (Figure 9C). The reason for that would be the next one. Given the bond strength of a dehydrogenated carboxylic group adsorbed on platinum in bidentate configuration, the rigidity of the backbone of the considered adsorbate, and the specific layouts of the platinum atoms exposed by the Pt(100)

and Pt(110) surfaces, an additional pair of platinum atoms to simultaneously bond the third carboxylic group in bidentate configuration is not accessible on these surfaces. Note that citrate would be already adsorbed on the surface through two dehydrogenated carboxylic groups simultaneously, each of them in bidentate configuration, However, on Pt(111), the atoms exposed by the surface are arranged in such a way as to enable the simultaneous adsorption of the three dehydrogenated carboxylic groups of citrate, each one of them in bidentate configuration. This adsorption mode has been already proposed for citrate on Au(111) analyzing STM images[58] or FTIR spectra.[55] However, other results indicate that dihydrogen citrate would be adsorbed in acid and neutral conditions, mainly in a monodentate configuration.[59] Those results were obtained using ex-situ conditions, in which water and bulk citrate species were removed from the sample. The elimination of water and citrate species may have altered the interfacial equilibria and the adsorption modes of citrate species, explaining the observed differences with the results presented here.

From the energetic in Table 1, it can be concluded that, under electrochemical conditions, citrate can be adsorbed on platinum through three dehydrogenated carboxylic groups simultaneously, each one of them in bidentate configuration, only on the Pt(111) surface at 0.54 V of potential (ΔG 1.63 eV), which coincides with the final stages of the adsorption process experimentally observed.

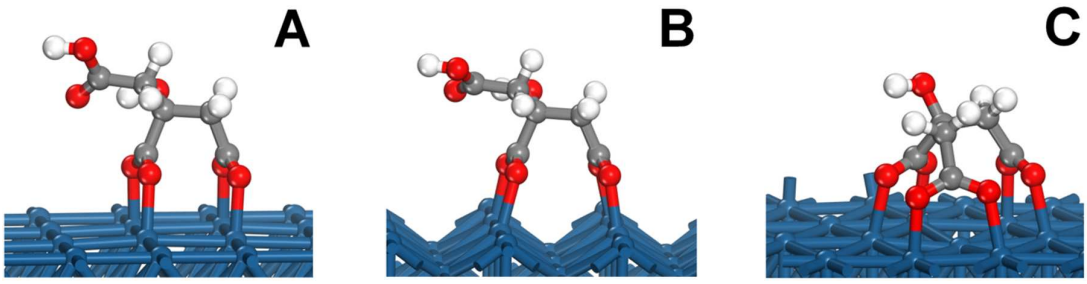

Figure 9. Adsorbed citrate on Pt(100) (A), Pt(110) (B) and Pt(111) (C) for the most favorable configuration found among those binding the higher number possible of carboxylic groups to the surface in bidentate form.

	Pt(100)		Pt(110)		Pt(111)	
	ΔG/eV	E/V	ΔG/eV	E/V	ΔG/eV	E/V
1 PCET	-0.25	-0.25	-0.73	-0.73	-0.19	-0.19
2 PCETs	0.24	0.12	-0.51	-0.26	0.66	0.33
3 PCETs	-	-	-	-	1.63	0.54

Table 1. Energetics (free energy ΔG and electrode potential E) of the adsorption processes of citrate on the different basal planes of platinum after one, two and three proton-coupled electron transfers (PCETs) under the dehydrogenated carboxylic groups bonded to the surface in bidentate configuration conditions.

3.3. Relationship between citrate and the shape of platinum colloidal NPs.

Because the adsorption behavior under electrochemical conditions can be related to the adsorption behavior in solution, the full set of the experimental and computational results reported here can be considered a consistent and reliable description of the adsorption properties of citrate on the different basal planes of platinum in water. The FTIR results prove that citrate can be strongly adsorbed on the Pt(111) surface in water through dehydrogenated carboxylic groups in bidentate configuration. This observation is consistent with the previous insight that the adsorption of acids lowers their pK_a, favoring their deprotonation.

Moreover, the charge numbers estimated from experiments point out that citrate can be adsorbed on the Pt(111) surface in water through two and three dehydrogenated carboxylic groups simultaneously, each one of them in bidentate configuration. The evidence supporting this assessment is multiple. First, plausible chemisorbed states of citrate on Pt(111) after two and three PCETs under the pre-established conditions were found using DFT. Second, the equilibrium potentials estimated from DFT for the citrate adsorption on Pt(111) are completely consistent with the experiments. Third, FTIR results indicate that the main chain of the adsorbed species lays parallel to the surface, a condition satisfied by all the found chemisorbed states. Finally, the simultaneous adsorption of the three carboxylic groups has been already proposed for citrate on the Au(111) electrode. It should be taken into account that nanoparticle synthesis is generally carried out in solutions where citrate is the main

species in solution. Under these conditions, and, owing to the higher K_a values of the adsorbed species, the only possible species adsorbed on the surface is citrate. Additionally, the adsorption isotherm show negligible dependence on the pH (figure 5). All these facts justify the extrapolation of the results obtained under acidic conditions to solutions with higher pH values.

On the other hand, as aforementioned, pieces of evidence of the adsorption modes of citrate on Pt(100) and Pt(110) cannot be directly obtained from experiments. However, on the one side, the comparison of the computational results obtained on Pt(111) with those obtained on Pt(100) and Pt(110) allows reasonably to establish that citrate can also be adsorbed on the Pt(100) and Pt(110) surfaces in water through two dehydrogenated carboxylic groups simultaneously, each one of them in bidentate configuration. On the other side, possible configurations of citrate adsorbed though three dehydrogenated carboxylic groups simultaneously, each one of them in bidentate configuration, could not be found on the Pt(100) and Pt(110) surfaces and, what is the most important, overwhelming geometric reasons have been given for that.

Additionally, the relative adsorption strength of each anion on each basal plane of platinum has been experimentally determined. It is found that citrate is more strongly adsorbed on all the platinum surfaces than acetate, which fact can be now easily explained. Because citrate can be adsorbed on these planes through two dehydrogenated carboxylic groups simultaneously, each one of them in bidentate configuration, instead of only one of them (the single one present in acetate), it is more strongly adsorbed than acetate. Unfortunately, the relative adsorption strength of citrate among the different basal planes of platinum could not be determined from qualitative comparisons.

At any case, the relevance of the adsorption mode of citrate in which the three carboxylic groups are simultaneously bonded to the surface in bidentate configuration, on the

Pt(111) surface, under certain synthesis conditions, can be established from the here reported results. On one side, according to our experimental and computational results, this adsorption mode of citrate on the Pt(111) surface under electrochemical conditions is favorable above ca. 0.5 V. On the other side, Pt nanoparticles are usually synthesized from $[PtCl_4]^{2+}$, whose standard potential for the reduction to Pt^0 is 0.73 V, which implies that Pt(II) ions are reduced at potentials below this value. The exact potential reached for the reduction process during the synthesis process will depend on the nature of the reductant species and the concentrations of this one and Pt(II) ions. However, it is clear that the lower the potential, the faster the reduction process will be. Thus, under controlled conditions, giving rise to low Pt reduction rates, the effective potential reached during the synthesis process will be close to the standard value, 0.73 V, ensuring the adsorption of citrate through the three carboxylic groups.

The detected adsorption behavior differences between the Pt(111) surface and the other two basal planes of platinum explain why colloidal nanoparticles of tetrahedral and octahedral shape are preferentially produced under certain conditions when citrate is used as the capping agent in water. If the shape of the NPs were determined only by the thermodynamics, all the NPs of fcc metals synthesized in absence of capping agents would have a cubo-octahedral shape (exhibiting (100) and (111) facets), since this configuration minimizes the surface energy.[60,61] This cubo-octahedral shape, and, more specifically, the ratio of (111) and (100) facets in the equilibrium shape, is determined by the relative surface energy of the (111), (100) and (110) planes. This ideal shape is difficult to obtain, because the growing process of the crystals is also affected by the kinetics.[23] It is generally accepted that a freshly deposited atom moves on the surface of the NP until it reaches a location where the energy is minimized. Under fast deposition conditions, the simultaneous interaction among several wandering atoms and the surface can trap them in sub-optimal locations, resulting in

rounded NPs without well-defined facets. Only under very controlled deposition conditions, NPs can attain a shape very close to his equilibrium shape, that is, the cube-octahedral shape.

The presence of capping agents modifies the thermodynamics and kinetics of the process, and under slow and controlled conditions, a preferential shape can be induced.[61] First, this equilibrium shape is determined by the relative surface energy of the different planes, and the presence of adsorbed species on them modifies the relative values of the planes. For the (111) plane, citrate bonds to 6 Pt surface atoms, implying a higher diminution of the surface energy than that obtained for the other two basal planes, where citrate only bonds to 4 atoms. Then, the lower energy of the (111) plane with respect to the (100) and (110) planes implies that the equilibrium shape of the nanoparticle would tend to have a higher ratio of (111) facets and a shape close to the perfect octahedral. On the other hand, kinetics effects can also operate on the mechanism. When the initial seed of the NP is formed, the small size of the nanocrystal (without well-defined facets) only allows the adsorption of citrate through a single carboxylic group. However, as the nanocrystal grows, the possible interaction of the free carboxylic groups of an adsorbed citrate with a Pt atom in the solution close to the surface will favor is faster deposition in a location that can be favorable for both the adsorbate and the substrate. Being the interaction of citrate larger on the Pt(111) surface, the described mechanism favors the formation of (111) facets, which leads to platinum NPs of tetrahedral and octahedral shape.

As aforementioned, the results obtained here for adsorbed citrate on platinum virtually match those reported for gold. In fact, the experimental evidence suggests that the adsorption behavior of different anions on the different fcc metals is almost identical. The examples in the literature are numerous. For instance, the adsorption of sulfate on (111) surfaces is similar for Pt, Rh, Au, Ir, Pd, Ir or Cu [62–68]. On all these surfaces, an identical rotated $\sqrt{3}\times\sqrt{7}$ surface

structure is observed for the adlayer of sulfate. Thus, it seems reasonable to assume that the here identified mechanism for citrate should also operate at least on pure fcc metals.

Finally, from the results reported here, a possible design principle for capping agents seems to emerge. To produce preferentially NPs of any shape, the adsorption modes of the capping agent on the different surfaces exposed by the growing crystals have to be thermodynamically and/or kinetically different enough. For certain adsorbable motifs and metals, such as the ones considered in this research (the carboxylic group on platinum), simple capping agents including a single adsorbable functional group would not be capable of giving rise to adsorption modes different enough. However, by incorporating several instances of a same absorbable motif to the supporting backbone of a more structurally complex capping agent, different enough adsorption modes can be potentially originated, depending on the specific surfaces exposed by the material. On the one side, bonding several functional groups to the surface, adsorption energies can potentially be increased. On the other side, the stretching, torsion, and bending of the backbone, required to enable the adsorption, would diminish them. Therefore, the final balance would depend on the specific surface exposed by the material.

4. Conclusions

The performance of advanced catalytic systems depends not only on the size and composition but also on the specific shape of the metal NPs from which many of them are assembled. Moreover, the shape of colloidal NPs depends on the substance used as the capping agent during their synthesis process. In turn, the action of capping agents is determined by their adsorption behavior on the different facets of the growing crystals whose shape they control. Unfortunately, the detailed adsorption properties of solvated species on the surfaces exposed by particles in suspension cannot be directly established. However, here

it is demonstrated that, from a careful combined reading of electrochemical experiments, FTIR spectra and DFT calculations, on well-defined surfaces, the adsorption behavior of capping agents on the surfaces exposed by metal NPs, during their synthesis process, can be reliably determined in sufficient detail to allow reasoning about the relationship between capping agents and NPs shapes. It is found that, because solvated citrate can become adsorbed on the Pt(111) surface through three dehydrogenated carboxylic groups simultaneously, each one of them in bidentate configuration, instead of only two, under the synthesis conditions, its interaction is stronger on the Pt(111) surface than on the other two basal planes of platinum. Although the experiments have been conducted in acid media, where the main bulk species is the citric acid, the adsorbed species is citrate, owing to the higher K_a values of adsorbed species. Thus, in neutral media, the described adsorption behavior explains why platinum colloidal nanoparticles of tetrahedral and octahedral shape are preferentially produced under certain conditions when citrate is used as the capping agent in water. But, the effort of untangle the mechanisms provides additional returns. From the understanding of the described mechanism regarding citrate, it can be reasoned that it should also operate determining the shape on other pure fcc metals. Additionally, the conceptualization of the identified mechanism suggests a design strategy which contributes to pave the way toward the engineering of specific capping agents for specific NP shapes. Finally, the way in which experimental and computational methods are here combined to determine adsorption properties of solvated species on particles in suspension could inspire future research.

ASSOCIATED CONTENT

Supporting Information

Supplemental Information includes supplemental experimental and computational procedures and figures, can be found at

Acknowledgments

This work has been financially supported by the MCINN-FEDER (Spain) through project CTQ2016-76221-P.

References

(1) Sun, C. Q.; Tay, B. K.; Zeng, X. T.; Li, S.; Chen, T. P.; Zhou, J.; Bai, H. L.; Jiang, E. Y. Bond-Order-Bond-Length-Bond-Strength (Bond-OLS) Correlation Mechanism for the Shape-and-Size Dependence of a Nanosolid. *J. Phys. Condens. Matter* **2002**, *14*, 7781–7795.

(2) Zanchet, D.; Tolentino, H.; Martins Alves, M. C.; Alves, O. L.; Ugarte, D. Inter-Atomic Distance Contraction in Thiol-Passivated Gold Nanoparticles. *Chem. Phys. Lett.* **2000**, *323*, 167–172.

(3) Koper, M. T. M. Structure Sensitivity and Nanoscale Effects in Electrocatalysis. *Nanoscale* **2011**, *3*, 2054–2073.

(4) Haruta, M. When Gold Is Not Noble: Catalysis by Nanoparticles. *Chem. Rec.* **2003**, *3*, 75–87.

(5) Li, Y.; Boone, E.; El-Sayed, M. A. Size Effects of PVP-Pd Nanoparticles on the Catalytic Suzuki Reactions in Aqueous Solution. *Langmuir* **2002**, *18*, 4921–4925.

(6) Link, S.; El-Sayed, M. A. Size and Temperature Dependence of the Plasmon Absorption of Colloidal Gold Nanoparticles. *J. Phys. Chem. B* **1999**, *103*, 4212–4217.

(7) Bard, A. J. Inner-Sphere Heterogeneous Electrode Reactions. Electrocatalysis and Photocatalysis: The Challenge. *J. Am. Chem. Soc.* **2010**, *132*, 7559–7567.

(8) Daniel, M.-C.; Astruc, D. Gold Nanoparticles: Assembly, Supramolecular Chemistry, Quantum-Size-Related Properties, and Applications toward Biology, Catalysis, and Nanotechnology. *Chem. Rev. (Washington, DC, United States)* **2003**, *104*, 293–346.

(9) Burda, C.; Chen, X.; Narayanan, R.; El-Sayed, M. A. Chemistry and Properties of Nanocrystals of Different Shapes. *Chem. Rev. (Washington, DC, United States)* **2005**, *105*, 1025–1102.

(10) Jia, C.-J.; Schüth, F. Colloidal Metal Nanoparticles as a Component of Designed Catalyst. *Phys. Chem. Chem. Phys.* **2011**, *13*, 2457.

(11) Sau, T. K.; Rogach, A. L. *Complex-Shaped Metal Nanoparticles : Bottom-up Syntheses and Applications*; Wiley-VCH, 2012.

(12) Sun, Y.; Xia, Y. Shape-Controlled Synthesis of Gold and Silver Nanoparticles. *Science (80-.).* **2002**, *298*, 2176 LP-2179.

(13) Ming, T.; Feng, W.; Tang, Q.; Wang, F.; Sun, L.; Wang, J.; Yan, C. Growth of Tetrahexahedral Gold Nanocrystals with High-Index Facets. *J. Am. Chem. Soc.* **2009**, *131*, 16350–16351.

(14) Sau, T. K.; Rogach, A. L. Nonspherical Noble Metal Nanoparticles: Colloid-Chemical Synthesis and Morphology Control. *Adv Mater* **2010**, *22*, *1781–1*, 1781–1804.

(15) Zeng, J.; Zheng, Y.; Rycenga, M.; Tao, J.; Li, Z. Y.; Zhang, Q.; Zhu, Y.; Xia, Y. Controlling the Shapes of Silver Nanocrystals with Different Capping Agents. *J. Am. Chem. Soc.* **2010**, *132*, 8552–8553.

(16) Turkevich, J.; Stevenson, P. C.; Hillier, J. A Study of the Nucleation and Growth Processes in the Synthesis of Colloidal Gold. *Discuss. Faraday Soc.* **1951**, *11*, 55–75.

(17) Turkevich, J.; Stevenson, P. C.; Hillier, J. The Formation of Colloidal Gold. *J. Phys. Chem.* **1953**, *57*, 670–673.

(18) Kimling, J.; Maier, M.; Okenve, B.; Kotaidis, V.; Ballot, H.; Plech, A. Turkevich Method for Gold Nanoparticle Synthesis Revisited. *J. Phys. Chem. B* **2006**, *110*, 15700–15707.

(19) Kumar, S.; Gandhi, K. S.; Kumar, R. Modeling of Formation of Gold Nanoparticles by Citrate Method. *Ind. Eng. Chem. Res.* **2007**, *46*, 3128–3136.

(20) Henglein, A.; Giersig, M. Formation of Colloidal Silver Nanoparticles: Capping Action of Citrate. *J. Phys. Chem. B* **1999**, *103*, 9533–9539.

(21) Ojea-Jiménez, I.; Bastús, N. G.; Puntes, V. Influence of the Sequence of the Reagents Addition in the Citrate-Mediated Synthesis of Gold Nanoparticles. *J. Phys. Chem. C* **2011**, *115*, 15752–15757.

(22) Ji, X.; Song, X.; Li, J.; Bai, Y.; Yang, W.; Peng, X. Size Control of Gold Nanocrystals in Citrate Reduction: The Third Role of Citrate. *J. Am. Chem. Soc.* **2007**, *129*, 13939–13948.

(23) Xia, Y.; Xiong, Y.; Lim, B.; Skrabalak, S. E. Shape-Controlled Synthesis of Metal Nanocrystals: Simple Chemistry Meets Complex Physics? *Angew. Chemie - Int. Ed.* **2009**, *48*, 60–103.

(24) Henglein, A.; Giersig, M. Reduction of Pt (II) by H2: Effects of Citrate and NaOH and Reaction Mechanism. *J. Phys. Chem. B* **2000**, *104*, 6767–6772.

(25) González-Peña, O. I.; Chapman, T. W.; Vong, Y. M.; Antaño-López, R. Study of Adsorption of Citrate on Pt by CV and EQCM. *Electrochim. Acta* **2008**, *53*, 5549–5554.

(26) Berkh, O.; Burstein, L.; Shacham-Diamand, Y.; Gileadi, E. The Chemical and Electrochemical Activity of Citrate on Pt Electrodes. *J. Electrochem. Soc.* **2011**, *158*, F85.

(27) Herrero, E.; Mostany, J.; Feliu, J. M.; Lipkowski, J. Thermodynamic Studies of Anion Adsorption at the Pt(111) Electrode Surface in Sulfuric Acid Solutions. *J. Electroanal. Chem.* **2002**, *534*, 79–89.

(28) Attard, G. A.; Hunter, K.; Wright, E.; Sharman, J.; Martínez-Hincapié, R.; Feliu, J. M. The Voltammetry of Surfaces Vicinal to Pt{110}: Structural Complexity Simplified by CO Cooling. *J. Electroanal. Chem.* **2017**, *793*, 137–146.

(29) Arán-Ais, R. M.; Figueiredo, M. C.; Vidal-Iglesias, F. J.; Climent, V.; Herrero, E.; Feliu, J. M. On the Behavior of the Pt(1 0 0) and Vicinal Surfaces in Alkaline Media. *Electrochim. Acta* **2011**, *58*, 184–192.

(30) Clavilier, J.; Albalat, R.; Gómez, R.; Orts, J. M.; Feliu, J. M.; Aldaz, A. Study of the Charge Displacement at Constant Potential During CO Adsorption on Pt(110) and Pt(111) Electrodes in Contact with a Perchloric Acid Solution. *J. Electroanal. Chem.* **1992**, *330*, 489–497.

(31) Clavilier, J.; Faure, R.; Guinet, G.; Durand, R. Preparation of Monocrystalline Pt Microelectrodes and Electrochemical Study of the Plane Surfaces Cut in the Direction of the {111} and {110} Planes. *J. Electroanal. Chem.* **1980**, *107*, 205–209.

(32) Herrero, E.; Orts, J. M.; Aldaz, A.; Feliu, J. M. Scanning Tunneling Microscopy and Electrochemical Study of the Surface Structure of Pt(10,10,9) and Pt(11,10,10) Electrodes Prepared Under Different Cooling Conditions. *Surf. Sci.* **1999**, *440*, 259–270.

(33) Delley, B. An Allelectron Numerical Method for Solving the Local Density Functional for Polyatomic Molecules An All-Electron Numerical Method for Solving the Local Density Functional for Polyatomic Molecules. *J. Chem. Phys. Addit. Inf. J. Chem. Phys. J. Homepage* **1990**, *92*, 508–517.

(34) Delley, B. Hardness Conserving Semilocal Pseudopotentials. *Phys. Rev. B* **2002**, *66*, 155125.

(35) Perdew, J. P.; Burke, K.; Ernzerhof, M. Generalized Gradient Approximation Made Simple [Phys. Rev. Lett. 77, 3865 (1996)]. *Phys. Rev. Lett.* **1997**, *78*, 1396.

(36) Hammer, B.; Hansen, L. B.; Nørskov, J. K. Improved Adsorption Energetics within Density-Functional Theory Using Revised Perdew-Burke-Ernzerhof Functionals. *Phys. Rev. B* **1999**, *59*, 7413–7421.

(37) Delley, B. From Molecules to Solids with the DMol(3) Approach. *J. Chem. Phys.* **2000**, *113*, 7756–7764.

(38) Tkatchenko, A.; Scheffler, M. Accurate Molecular Van Der Waals Interactions from Ground-State Electron Density and Free-Atom Reference Data. *Phys. Rev. Lett.* **2009**, *102*, 73005.

(39) Delley, B. The Conductor-like Screening Model for Polymers and Surfaces. *Mol. Simul.* **2006**, *32*, 117–123.

(40) Neugebauer, J.; Scheffler, M. Adsorbate-Substrate and Adsorbate-Adsorbate Interactions of Na and K Adlayers on Al(111). *Phys. Rev. B* **1992**, *46*, 16067–16080.

(41) Nørskov, J. K.; Rossmeisl, J.; Logadottir, A.; Lindqvist, L.; Kitchin, J. R.; Bligaard, T.; Jónsson, H. Origin of the Overpotential for Oxygen Reduction at a Fuel-Cell Cathode. *J. Phys. Chem. B* **2004**, *108*, 17886–17892.

(42) Attard, G. A.; Ye, J. Y.; Jenkins, P.; Vidal-Iglesias, F. J.; Herrero, E.; Sun, S. G. Citrate Adsorption on Pt{hkl} Electrodes and Its Role in the Formation of Shaped Pt Nanoparticles. *J. Electroanal. Chem.* **2013**, *688*, 249–256.

(43) Savich, W.; Sun, S. G.; Lipkowski, J.; Wieckowski, A. Determination of the Sum of Gibbs Excesses of Sulfate and Bisulfate Adsorbed at the Pt(111) Electrode Surface Using Chronocoulometry and Thermodynamics of the Perfectly Polarized Electrode. *J. Electroanal. Chem.* **1995**, *388*, 233–237.

(44) Herrero, E.; Mostany, J.; Feliu, J. M.; Lipkowski, J. Thermodynamic Studies of Anion Adsorption at the Pt(111) Electrode Surface in Sulfuric Acid Solutions. *J. Electroanal. Chem.* **2002**, *534*, 79–89.

(45) Mostany, J.; Herrero, E.; Feliu, J. M.; Lipkowski, J. Thermodynamic Studies of Anion Adsorption at Stepped Platinum(Hkl) Electrode Surfaces in Sulfuric Acid Solutions. *J. Phys. Chem. B* **2002**, *106*, 12787–12796.

(46) Garcia-Araez, N.; Climent, V.; Herrero, E.; Feliu, J.; Lipkowski, J. Thermodynamic

Studies of Chloride Adsorption at the Pt(1 1 1) Electrode Surface from 0.1 M HClO4 Solution. *J. Electroanal. Chem.* **2005**, *576.*

(47) Garcia-Araez, N.; Climent, V.; Herrero, E.; Feliu, J. M.; Lipkowski, J. Thermodynamic Approach to the Double Layer Capacity of a Pt(111) Electrode in Perchloric Acid Solutions. *Electrochim. Acta* **2006**, *51*, 3787–3793.

(48) Mostany, J.; Martínez, P.; Climent, V.; Herrero, E.; Feliu, J. M. Thermodynamic Studies of Phosphate Adsorption on Pt(111) Electrode Surfaces in Perchloric Acid Solutions. *Electrochim. Acta* **2009**, *54*, 5836–5843.

(49) Garcia-Araez, N.; Climent, V.; Rodríguez, P.; Feliu, J. M. Thermodynamic Analysis of (Bi)Sulphate Adsorption on a Pt(111) Electrode as a Function of PH. *Electrochim. Acta* **2008**, *53*, 6793–6806.

(50) Garcia-Araez, N.; Climent, V.; Rodriguez, P.; Feliu, J. M. Elucidation of the Chemical Nature of Adsorbed Species for Pt(111) in H2SO4 Solutions by Thermodynamic Analysis. *Langmuir* **2010**, *26*, 12408–12417.

(51) Parsons, R.; Trasatti, S. Interphases in Systems of Conducting Phases. *J. Electroanal. Chem.* **1986**, *205*, 359–376.

(52) Martinez-Hincapie, R.; Berna, A.; Rodes, A.; Climent, V.; Feliu, J. M. Surface Acid-Base Properties of Anion-Adsorbed Species at Pt(111) Electrode Surfaces in Contact with CO2-Containing Perchloric Acid Solutions. *J. Phys. Chem. C* **2016**, *120*, 16191–16199.

(53) Martínez-Hincapié, R.; Sebastián-Pascual, P.; Climent, V.; Feliu, J. M. Exploring the Interfacial Neutral PH Region of Pt(111) Electrodes. *Electrochem. Commun.* **2015**, *58*, 62–64.

(54) Kunze, J.; Burgess, I.; Nichols, R.; Buess-Herman, C.; Lipkowski, J. Electrochemical Evaluation of Citrate Adsorption on Au(1 1 1) and the Stability of Citrate-Reduced Gold Colloids. *J. Electroanal. Chem.* **2007**, *599*, 147–159.

(55) Nichols, R. J.; Burgess, I.; Young, K. L.; Zamlynny, V.; Lipkowski, J. A Quantitative Evaluation of the Adsorption of Citrate on Au(1 1 1) Using SNIFTIRS. *J. Electroanal. Chem.* **2004**, *563*, 33–39.

(56) Rodes, A.; Pastor, E.; Iwasita, T. An Ftir Study on the Adsorption of Acetate at the Basal Planes of Platinum Single-Crystal Electrodes. *J. Electroanal. Chem.* **1994**, *376*, 109–118.

(57) Pastor, E.; Rodes, A.; Iwasita, T. Spectroscopic Investigations on the Adsorption of Trifluoracetate at P t(100), Pt(110) and Pt(111). *J. Electroanal. Chem.* **1996**, *404*, 61–68.

(58) Lin, Y.; Pan, G.-B.; Su, G.-J.; Fang, X.-H.; Wan, L.-J.; Bai, C.-L. Study of Citrate Adsorbed on the Au(111) Surface by Scanning Probe Microscopy. *Langmuir* **2003**, *19*, 10000–10003.

(59) Park, J.-W.; Shumaker-Parry, J. S. Structural Study of Citrate Layers on Gold Nanoparticles: Role of Intermolecular Interactions in Stabilizing Nanoparticles. *J. Am. Chem. Soc.* **2014**, *136*, 1907–1921.

(60) Aiken, J. D.; Finke, R. G. A Review of Modern Transition-Metal Nanoclusters: Their Synthesis, Characterization, and Applications in Catalysis. *Journal of Molecular Catalysis A: Chemical*. Elsevier September 8, 1999, pp 1–44.

(61) Barmparis, G. D.; Lodziana, Z.; Lopez, N.; Remediakis, I. N. Nanoparticle Shapes by Using Wulff Constructions and First-Principles Calculations. *Beilstein Journal of Nanotechnology*. Beilstein-Institut February 3, 2015, pp 361–368.

(62) Funtikov, A. M.; Linke, U.; Stimming, U.; Vogel, R. An In-Situ STM Study of Anion Adsorption on Pt(111) from Sulfuric Acid Solutions. *Surf. Sci.* **1995**, *324*, L343–L348.

(63) Wan, L. J.; Yau, S. L.; Itaya, K. Atomic-Structure of Adsorbed Sulfate on Rh(111) in Sulfuric- Acid-Solution. *J. Phys. Chem.* **1995**, *99*, 9507–9513.

(64) Magnussen, O. M.; Hageböck, J.; Hotlos, J.; Behm, R. J. In Situ Scanning Tunnelling Microscopy Observations of a Disorder-Order Phase Transition in Hydrogensulfate Adlayers on Au(111). *Faraday Discuss.* **1992**, *94*, 329–338.

(65) Wan, L. J.; Suzuki, T.; Sashikata, K.; Okada, J.; Inukai, J.; Itaya, K. In Situ Scanning Tunneling Microscopy of Adsorbed Sulfate on Well-Defined Pd(111) in Sulfuric Acid Solution. *J. Electroanal. Chem.* **2000**, *484*, 189–193.

(66) Wan, L. J.; Hara, M.; Inukai, J.; Itaya, K. In-Situ Scanning Tunneling Microscopy of Well-Defined Ir(111) Surface: High-Resolution Imaging of Adsorbed Sulfate. *J. Phys. Chem. B* **1999**, *103*, 6978–6983.

(67) Kim, Y. G.; Soriaga, J. B.; Vigh, G.; Soriaga, M. P. Atom-Resolved EC-STM Studies of Anion Adsorption at Well-Defined Surfaces: Pd(111) in Sulfuric Acid Solution. *J. Colloid Interface Sci.* **2000**, *227*, 505–509.

(68) Li, W. H.; Nichols, R. J. An in Situ Stm Study of Sulphate Adsorption on Copper(111) in Acidic Aqueous Electrolytes. *J. Electroanal. Chem.* **1998**, *456*, 153–160.

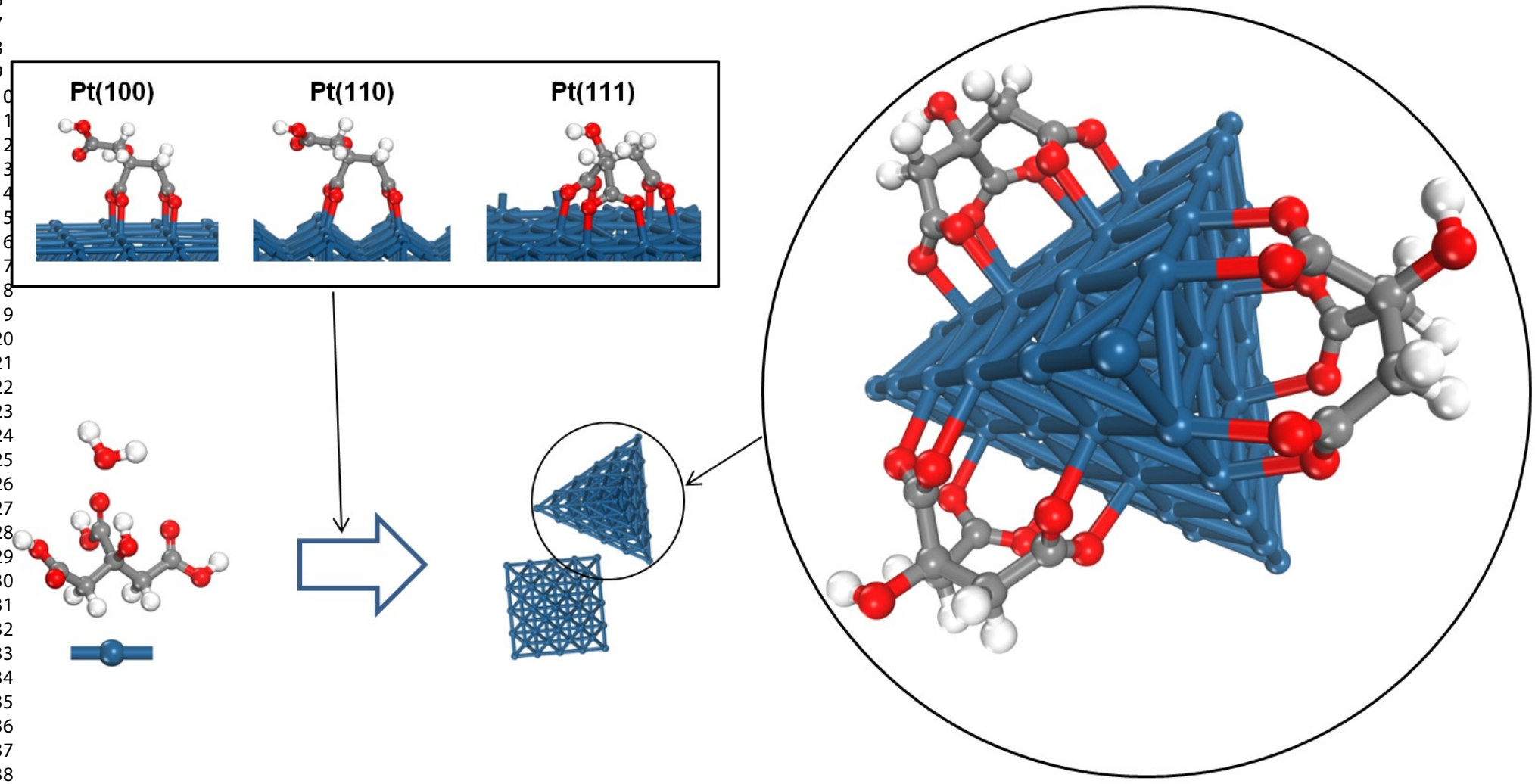
Pt(100)
Pt(110)
Pt(111)